Transformer-Based Approach for Predicting Transactive Energy in Neurorehabilitation

Naveed Ahmad Khan, Tanishka Goyal, Fahad Hussain, Prashant K. Jamwal, *Senior Member, IEEE*, and Shahid Hussain

***Abstract*— Advancements in robotic neurorehabilitation have made it imperative to enhance the safety and personalization of physical human-robot interactions (pHRI). Estimation and management of energy transfer between humans and robots is essential for enhancing safety during the rehabilitation. Traditional control methods, which rely on coordinate-based monitoring of robot velocity and external forces, often fail in unstructured environments due to their susceptibility to sensor noise and limited adaptability to individual patient needs. This paper introduces the concept of transactive energy, a coordinate-invariant entity that captures the energy dynamics between the human and the robot during robot-assisted rehabilitation and can be used for personalized robot control. However, estimation of such energy transfer is a complex process and therefore, we have developed a transformer-based model to predict the transactive potential energy. The proposed model is implemented on an ankle rehabilitation robot which is a compliant parallel robot and provides the required three rotational degrees of freedom (DOF). The model learns from the data obtained from the experiments carried out using the ankle robot with five stroke patients on two types of controllers: an impedance controller operated in zero impedance control mode and a trajectory tracking controller. This study provides a baseline, for future research on energy-based control mechanisms in pHRI applications, by utilizing the advanced deep learning models.**

***Index Terms*— Transactive energy, neurorehabilitation, energy transfer, physical human–robot interaction, transformer model, adaptive learning.**

Received 11 August 2024; revised 11 October 2024 and 10 November 2024; accepted 6 December 2024. Date of publication 11 December 2024; date of current version 17 December 2024. The work of Naveed Ahmad Khan was supported by Australian Government Research Training Program (RTP) Scholarship through the University of Canberra. The work of Prashant K. Jamwal was supported by Nazarbayev University, Kazakhstan, under the Faculty-Development Competitive Research Grants Program for 2024–2026 under Grant 201223FD8813. *(Corresponding author: Naveed Ahmad Khan.)*

This work involved human subjects or animals in its research. Approval of all ethical and experimental procedures and protocols was granted by the Institutional Research and Ethics Committee (IREC) of Nazarbayev University under Application No. 683/27022023.

Naveed Ahmad Khan, Tanishka Goyal, Fahad Hussain, and Shahid Hussain are with the School of Information Technology and Systems, University of Canberra, Canberra, ACT 2617, Australia (e-mail: naveedahmad.khan@canberra.edu.au).

Prashant K. Jamwal is with the Department of Electrical and Computer Engineering, Nazarbayev University, Astana 010000, Kazakhstan.

Digital Object Identifier 10.1109/TNSRE.2024.3515175

I. Introduction

THE synergistic integration of technology and artificial intelligence (AI) has significantly advanced the development of intelligent robots [1]. Modern robots are being developed with human-like intelligence, facilitating the complex human-robot interaction based on mechanical energy. These advancements have major implications for rehabilitation, especially for patients with mobility impairment [2]. Ankle robots, for instance, are designed for the treatment of ankle disorders and have demonstrated great potential in assisting patients by offering targeted assistance to the lower limb and facilitating the recovery of gait function through controlled mechanical energy inputs [3]. The ankle joint complex (AJC) is a highly complex anatomical structure that supports movements in three DOF: inversion/eversion (IN/EV), dorsiflexion/plantarflexion (DO/PL), and adduction/abduction (AD/AB) [4]. Neurological injuries, particularly stroke, often result in ankle dysfunctions such as drop foot, ankle clonus, spasticity, toe walking, etc. Stroke causes substantial disabilities worldwide, with more than 15 million new stroke cases each year and 50 million stroke survivors [5]. Increasing stroke incidences and resulting disabilities have led to advancements in robot-assisted ankle rehabilitation, aiming to deliver effective rehabilitation to a larger population with a limited number of available therapists.

The advancements in rehabilitation technology over the past two decades are driven by the need to provide effective rehabilitation solutions for patients with lower limb impairments. Notably, the Rutgers ankle rehabilitation system utilizes the Stewart platform to accurately control ankle movements in all three DOF [6]. This system has proven its potential to improve rehabilitation outcomes by delivering accurate and consistent therapeutic exercises. Building on this, the MIME (Mirror Image Movement Enabler) robot was designed to help stroke patients regain motor functions by replicating the movements of the unaffected limb to the affected limb [7], [8]. Furthermore, the advancements were made by the Lokomat robotic gait trainer, providing body-weight-supported treadmill training, which aids in the recovery of walking abilities in patients with neurological impairments [9]. The MIT-Manus robot, originally designed for upper limb rehabilitation, has been adapted for ankle rehabilitation using repetitive and adaptive training protocols, illustrating its versatility in therapeutic

contexts and its capability to deliver effective rehabilitation interventions across different patient needs [10]. Several other mechanisms have been developed including the Anklebot, designed by Roy et al. [11], featuring soft robotics, integrating force feedback, real-time motion analysis, and offering adaptable support that replicates the natural ankle movements. The ReSTORE exosuit uses a soft, lightweight design to assist with plantarflexion and dorsiflexion reducing injury risk, and enhancing patient comfort during rehabilitation [12].

In recent times, the parallel ankle rehabilitation robots (PARRs), due to their unique mechanical designs and advanced actuation systems have established themselves as a superior alternative to traditional exoskeletons and powered orthoses, as they offer adjustable resistance and assistive forces to facilitate wide range of ankle exercises [13]. Chang and Zhang [14] developed a parallel mechanism for rehabilitation by addressing the challenge of motion decoupling by incorporating three degrees of freedom to facilitate a more natural and comprehensive range of motions. Further advancements were made by Zhao et al. [15] that focused on improving the stiffness and carrying capacity of parallel robotic systems. Their finding highlights the necessity of balancing mechanical flexibility with structural stability to achieve optimal results. The incorporation of virtual reality with the Walkbot robot was investigated by Lee et al. [16]. It allows the integration of customized and adaptive rehabilitation exercises by creating VR environments to simulate various walking conditions and terrains.

The advancements in ankle rehabilitation robots have not only focused on mechanical design but also on the development of control strategies to enhance human-robot interaction. Impedance control has been extensively studied due to its dynamic modulation to adjust the stiffness and damping properties of the mechanisms. Remarkably, a variable impedance controller introduced by Arnold and Lee [17] dynamically modulates both stiffness and damping to improve the trade-off between stability and agility in coupled human-robot systems by adjusting robotic damping from negative to positive values to either inject or dissipate energy based on the indented motion of the patient and also estimates the direction to apply a variable stiffness torque, stabilizing the user towards an optimal trajectory. Perez-Ibarra et al. [18] propose an assistive-resistive approach by adapting the stiffness parameter of the robot's impedance control to optimize the balance between stability and flexibility for enhancing active patient participation during robotic therapy through real-time adaptation of robotic assistance based on the patient's instantaneous participation and performance. Zhang et al. [19] extend the interconnection and damping assignment passivity-based control (IDA-PBC) framework to a hip exoskeleton, enabling task-invariant assistance by optimizing torque based on natural human movement. Qian et al. [20] applied iterative learning to impedance control allowing robots to adjust their impedance models based on repeated interaction tasks. Han et al. [21] employed deep reinforcement learning to create an impedance control strategy, where the robot learned optimal settings through patient interactions to enhance therapy efficacy and comfort. Li et al. [22] proposed a novel hybrid impedance controller with an adaptive radial basis function neural networks to manage the nonlinear and variable nature of human-robot interactions during rehabilitation. Wang et al. [23] successfully employed the Proportional-Integral-Derivative (PID) control to achieve accurate and precise torque and control joint angles to acknowledge the need of patients. The fuzzy logic controller, designed by Abayneh [24] was used to address the complexities, uncertainties, and nonlinearities in robot control. These advancements in control methodologies have enabled the development of rehabilitation robots, offering improved recovery and better rehabilitation to patients suffering from ankle disorders.

Building on the innovations in designs and controller algorithms for rehabilitation robots, the concept of transactive energy has garnered increasing attention due to its potential to optimize the interaction and the dynamic exchange of mechanical energy between the robot and the human subject [25]. The exchange of energy during physical interaction provides a coordinate-invariant measure that may enhance the adaptability of robots [26]. Since the early 1980s, energy-shaping techniques have been used to preserve passivity in robotic systems to ensure safe interactions [27]. In rehabilitation, controlling the energy exchange is most important due to variability in the force and movements. Lee and Hogan [28] studied the need for precise energy management to ensure stability and optimize performance in rehabilitation. They highlighted that effective control of the total energy (including Kinetic and potential energy) in an impendence-controlled robot could effectively reduce the risks associated with unstructured environments like clamping scenarios or unexpected collisions. Recently, energy shaping methods have been used as a promising tool for optimizing human-robot interactions in powered exoskeletons to provide task-invariant assistance by altering the dynamic characteristics of the human body [29], [30]. Lin et al. [31] presented a novel control method that combines energy shaping with a machine learning-based classifier to optimize task-agnostic assistance in powered exoskeletons by dynamically adjusting energy shaping controllers based on classified task and gait patterns, which improves the exoskeleton's adaptability and enhances the alignment of human joint moments across various activities. Moreover, Lachner et al. [32] introduced an energy budgeting approach that specifies a particular energy value for each control cycle to balance the need for sufficient energy for tasks and minimize injury risks from unintended interactions. This technique not only enhances safety but also simplifies the certification process for physical human-robot interaction by reducing the number of safety-related parameters to a single energy value, streamlining the traditional certification process that involves extensive and complicated steps such as virtual set-up in simulation, installation and programming of the robot, risk assessments, and verification of impact forces with measurement devices. Dietrich et al. [33] proposed the "energy tank" concept, which restricts the robot's energy to a finite amount to ensure both safe and stable operation in dynamic and unpredictable settings.

These traditional energy management techniques have improved safety and stability in rehabilitation robots, but they rely on predefined energy limits and control cycles, which constrain their adaptability to the dynamic and individualized nature of pHRI. This static nature of energy often results in either under-utilization or excessive energy transfer. Therefore, in this paper, we present the novel concept of transactive energy as a means to optimize energy exchanges between robots and humans during ankle rehabilitation. It emphasizes the importance of balancing energy transfer which enables the robot to continuously adapt its energy exchange to the specific and evolving needs of the patient during therapy. This approach allows to precisely monitor how energy is transferred within the system, including the energy exerted by the human and the energy exchanged between the human and the robot.

Furthermore, we investigate the concept of transactive energy using AI techniques such as a transformer model to improve human-robot interactions by predicting and managing the dynamic exchange of energy during rehabilitation. The transformer model is chosen for its exceptional ability to handle sequential data and capture long-term dependencies, which is important for estimating the energy exchanges over time. Traditional methods and other neural network models face several drawbacks when managing the nonlinear and dynamic nature of transactive energy. The real-time fluctuations in energy during human-robot interaction add a high level of complexity to this task. For instance, in active mode, the energy can fluctuate rapidly as the robot responds to the patient's varying levels of exertion. In such cases, traditional methods like the Ziegler-Nichols Method, and Tyreus-Luyben Method for tuning PID control often lack flexibility, while neural network models such as recurrent neural networks and conventional neural networks can be slow to train and deploy [34], [35]. These models may also require significant adaptation to handle time-series data, increasing computational costs and complexity considerably [36]. Therefore, it is necessary to explore more advanced techniques that offer real-time adaptability and precise control over the nonlinear and dynamic aspects of transactive energy distribution. Recently, the transformer models have demonstrated their generalization capabilities across various domains encouraging us to implement them for effectively managing and estimating transactive energy in human-robot interactions. These models employ a multi-head self-attention mechanism, that allows the model to simultaneously focus on different parts of the input sequence and reducing the risk of overfitting and ensuring robust performance [37].

This paper is organized as follows: Section II highlights the detailed methodology including the introduction to the mathematical framework for the transactive energy and the proposed transformer model for the prediction of the energies followed by the results and discussion in section III. The conclusion drawn from the work is presented in section IV.

II. Methodology

A. Parallel Ankle Rehabilitation Robot

In this study, we have utilized the adaptive wearable parallel ankle rehabilitation robot developed by Jamwal et al. [38], which is designed to facilitate physical rehabilitation for ankle injuries. The robot's bio-inspired design includes lightweight yet robust PMAs that provide the necessary actuation to achieve three rotational DOFs to simulate the action of skeletal muscles as shown in Figure 1. The ankle rehabilitation robot operates through mechanical and control components equipped with PMAs that contract or expand in response to controlled air pressure, generating movement in the ankle joint. The robot's functioning is based on both passive and active control modes, where the robot can either assist the patient in performing movements or follow the patient's motions. The robot's functionality is further enhanced by a series of sensors that monitor various parameters such as joint angles, force applied, and the position of the ankle. These sensors relay information to the control system, which adjusts the actuators to maintain safe and effective motion. The details of the ranges of the motion are presented in Table I.

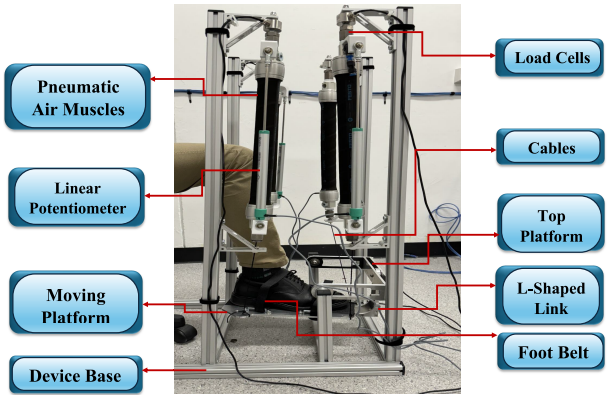

Fig. 1. Illustration of the experimental setup for parallel ankle rehabilitation robot with a healthy subject.

TABLE I
Robot Capabilities for Different Types of Motion [38]

Type of motion	Required Range	Maximum motion	Moment capacity
Abduction	15.4° – 25.9°	52°	68 Nm
Adduction	22° – 36°	52°	68 Nm
Eversion	10° – 17°	26°	96 Nm
Inversion	14.5° – 22°	26°	96 Nm
Plantarflexion	37.6° – 45.75°	46°	120 Nm
Dorsiflexion	20.3° – 29.8°	46°	120 Nm

In [38] the initial design and mathematical modeling are detailed to highlight the adaptability and the use of PMAs to provide compliant actuation to understand their behavior and interaction with the human ankle joint. Furthermore, the control strategies are explored in [39], which focused on the adaptive fuzzy logic controller and a fuzzy-based disturbance observer (FBDO) to manage the nonlinear features of PMAs. These control strategies were validated through experiments with a neurologically intact subject, demonstrating the robot's ability to simultaneously control four parallel actuators, exhibiting effective trajectory tracking and enhanced patient engagement during rehabilitation. Readers are referred to [40], [41], and [42] for

further details regarding the parallel ankle rehabilitation robot mechanism.

B. Velocity Mapping and Contact Force Analysis

In this section, we discuss the mathematical foundation for managing the energy dynamics of a robotic system involved in physical human-robot interaction. Initially, focusing on the Jacobian matrix and the estimation of external forces, which provides the kinematic relationships and force dynamics essential for understanding the system's behavior. The Jacobian matrix $\mathbf{H}(\theta) \in \mathbb{R}^{p\times k}$ encapsulates the robot's structure and kinematic configuration by linking the joint space velocities to the Cartesian space velocities, it provides translation of desired end-effector's position into the corresponding joint movements θ required to achieve them by following equation:

$$\mathbf{U} = \mathbf{H}(\theta)\dot{\theta}, \tag{1}$$

here, $\mathbf{U} \in \mathbb{R}^p$ is a vector of Cartesian velocities of linear and angular components of the end-effector, and $\dot{\theta} \in \mathbb{R}^k$ is a vector of velocities of joint variables. p and k are the number of Cartesian coordinates and number of joint variables respectively. The $\mathbf{H}(\theta)$ defined in Eq. (2) encapsulates the sensitivity of the actuator lengths to changes in the Euler angles that involves partial derivatives of the rotation matrix with respect to each Euler angle, which captures the changes in the joint configuration affecting both the translational and rotational components of the actuator positions as [43]:

$$\mathbf{H}(\theta) = \begin{bmatrix} \frac{\partial \xi_1}{\partial \theta_x} & \frac{\partial \partial \xi_1}{\partial \theta_y} & \frac{\partial \partial \xi_1}{\partial \theta_z} \\ \vdots & \vdots & \vdots \\ \frac{\partial \xi_4}{\partial \theta_x} & \frac{\partial \xi_4}{\partial \theta_y} & \frac{\partial \xi_4}{\partial \theta_z} \end{bmatrix}, \tag{2}$$

where each element can be obtained using Eq. (3):

$$\frac{\partial \xi_i}{\partial \theta_k} = \frac{1}{\xi_i}\left(\frac{\partial \mathbf{R}(\theta)}{\partial \theta_k}\mathbf{P}_i\right)^{\top}(\mathbf{R}(\theta)\mathbf{P}_i + (\mathbf{t} - \mathbf{B}_i)), \tag{3}$$

here, $\mathbf{B}_i$ and $\mathbf{P}_i$ are the base point and local position vector of the $i-th$ actuator, t is translational offset of the system and $\mathbf{R}(\theta)$ is the rotation matrix constructed from the Euler angles. In kinematically redundant systems, numerous possible joint velocity configurations can achieve the same desired Cartesian velocity. For example, the corresponding joint velocities for a given end-effector velocity are not uniquely defined which can lead to an increase in the joint velocities, which may create an unsafe environment for the human subject. Therefore, to lower the impact of a collision, often a load cells are used to detect joint torques that identify contact with the environment by calculating the difference between the measured and control torques. This approach is highly dependent on precise model data and the robot's configuration and it struggles to distinguish between intentional and accidental interactions. Therefore, the inverse of the Jacobian matrix is utilized in estimating the relationship between the external forces and joint torques [32]. The external forces $\hat{\mathbf{F}}_{\mathbf{ext}} \in \mathbb{R}^p$ acting on a robot structure are calculated using Eq. (4) by mapping the external torques $\hat{\Gamma}_{\mathbf{ext}} \in \mathbb{R}^k$ into Cartesian space as:

$$\hat{\Gamma}_{\mathbf{ext}} = \left(\mathbf{H}(\theta)^{-1}\right)^T \hat{\Gamma}_{\mathbf{ext}}. \tag{4}$$

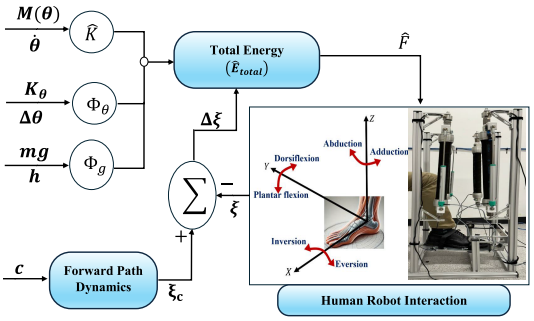

Fig. 2. Norton equivalent network for the dynamics of human-robot interaction. Here, $\hat{K}$ is kinetic energy, Φ_g is gravitational potential energy, and Φ_θ shows controlled potential energy based on orientation in Cartesian space.

C. Energy Transfer During Interaction

In pHRI, it is important to study the dynamics of transactive energy to maintain efficiency and safety. The environmental interaction of the ankle robot that exhibits the mechanical impedance behavior can be modeled as an equivalent network as shown in Figure 2. It shows the dynamics at the interaction point $(\hat{\mathbf{F}}, \mathbf{U})$ and models the calculation of the force applied by the robot and the displacement influenced by the human subject, ensuring that the robot can respond appropriately to the human's actions for safe and effective collaboration [44]. The robot controller determines the desired motion $\xi_a \in \mathbb{R}^3$. The energy flow is bi-directional, and if the robot is considered as mechanical impedance, the force $\hat{\mathbf{F}}$ will be the output for displacement ξ which can be considered as the input. In such case the total energy $\hat{\mathbf{E}}_{\mathbf{total}}$ defined in Eq. (5) of the robotic system is [32]:

$$\hat{\mathbf{E}}_{\mathbf{total}} = \hat{K}(\dot{\theta}, M(\theta)) + \Phi_g(\theta) + \Phi_\xi(\Delta\xi, K_\xi) + \Phi_\theta(\Delta\theta, K_\theta). \tag{5}$$

Here, $\hat{K}$ is kinetic energy, Φ_g is gravitational potential energy, and $\Phi_\theta, \Phi_\xi, \in \mathbb{R}$ shows controlled potential energy based on orientation in Cartesian space and potential energy based on joint positions in joint space respectively. These energies are defined as [45]:

$$\hat{K} = \frac{1}{2}\dot{\theta}^T M(\theta)\dot{\theta}, \quad \Phi_g = mgh(\theta),$$
$$\Phi_\xi = \frac{1}{2}(\Delta\xi)^T K_\xi(\Delta\xi).$$

When the robot starts to move, the potential energies including gravitational potential energy, potential energy in Cartesian space, and potential energy due to joint positions are transferred as kinetic energy. This kinetic energy is then delivered to the human subject and is directly proportional to the mass of robot $M(\theta)$ and the velocity of joints. The robot's configuration is directly related to Φ_g and it is essential to compensate robot's instantaneous weight, which fluctuates due to the continuous expansion and contraction of the PMAs. The potential energy based on orientation Φ_θ is a function of the stiffness $K_\theta = \frac{\hat{\mathbf{F}}_{\mathbf{int}}}{\Delta\theta} \in \mathbb{R}^{p\times p}$, dependent on interaction force $\hat{\mathbf{F}}_{\mathbf{int}}$, and the orientation error $\Delta\theta = (\theta_c - \theta) \in \mathbb{R}^p$, where θ_c is the desired position and θ is the actual position [32].

Similarly, Φ_ξ is varied by the stiffness matrix $K_\theta = \frac{\hat{\Gamma}_{\mathbf{int}}}{\Delta\xi} \in \mathbb{R}^{n\times n}$ of joints and the difference in joint positions $\Delta\xi = (\xi_c - \xi) \in \mathbb{R}^k$, with ξ_c representing the desired joint positions, ξ shows the actual joint positions and $\hat{\Gamma}_{\mathbf{int}}$ is the interaction torque. Both ξ_c and θ_c are functions of the control time $t_c \in \mathbb{R}$ [46]. For Cartesian space, various methods have been developed to describe the impedance potential. The total potential energy in the coordinate frame is defined as:

$$\Phi_\theta = \Phi_p + \Phi_\epsilon, \tag{6}$$

where Φ_p and Φ_ϵ are translational and rotational potential energies and they are typically functions of the robot's stiffness, translational error, and orientation errors. From Eq. (6), the control torques $\hat{\Gamma}$ defined in Eq. (7) can be derived as the partial derivatives of translational and rotational potential energies, for the system's generalized position and joint coordinates as:

$$\hat{\Gamma} = (\mathbf{H}(\theta))^T \left(\frac{\partial\Phi_\xi}{\partial\xi}\right) + \left(\frac{\partial\Phi_\theta}{\partial\theta}\right). \tag{7}$$

To accomplish the required impedance control, these gradients supply the required torques, enabling the robot to react dynamically to the motions of the human subject. In addition to the energy transfer dynamics from the robot to the human, we have further discussed the patient's engagement during the rehabilitation exercises by formulating the the work done (W) model. The energy transfer in the form of work done from the human to the robot during the interaction can be given by Eq. (8):

$$W = \sum_{x=1}^{n-1} \frac{P_x + P_{x+1}}{2} \cdot (t_{x+1} - t_x), \tag{8}$$

here, P is instantaneous power at $x - th$ time.

D. Impedance Control

Transactive energy, which involves the exchange of energy flow between the human and the robot, is an important aspect of implementing impedance control in rehabilitation robotics. The two control modes designed for the given parallel ankle rehabilitation robot have been previously discussed in [39] and [47]. In trajectory tracking control mode, the ankle robot was actuated while the patients were asked to remain completely inactive. The robot directed the subject's ankle along specified trajectories, focused on reducing tracking errors. Zero-Impedance Control Mode allowed the robot to remain passive, giving subjects maximum freedom to move their ankles.

E. Experimental Protocol

The performance of the aforementioned controllers was evaluated in five mildly impaired stroke patients (aged 28-52) (four male and one female) who were 4-6 months post-stroke. Ethics approval for this study was obtained from the Institutional Research and Ethics Committee (IREC) of Nazarbayev University for all experiments involving human subjects. We hypothesized that the pattern of energy transfer during physical human-robot interaction would differ significantly between passive and active phases, impacting the overall efficiency and safety of the interaction. To test this hypothesis, we designed an experimental protocol with two sets of experiments conducted with stroke survivors: in the first set, subjects remained passive for 15 minutes and then actively tracked the reference trajectories for the next 15 minutes; in the second set, subjects actively tracked the reference trajectories for the first 15 minutes and then remained passive for the subsequent 15 minutes. The data recorded during the experiments include actuator displacements measured by linear potentiometers, forces measured by a load cell, and the joint angles, showing the ankle's movements in flexion, inversion-eversion, and adduction-abduction. In addition, the lengths of the actuators and orientations of the end-effector were also recorded.

F. Transformer Model

In this work, we have implemented the transformer model for the unsupervised predictions of the potential energies (Φ_ξ, Φ_θ) based on given inputs like Euler angles and actuator lengths of the actuators of ankle rehabilitation robot during the human-robot interactions. The transformer models were introduced by Vaswani et al. [48] that rely on self-attention mechanisms to process input and output sequences. This model facilitates parallelization during training, which leads to significant improvements in computational efficiency and scalability of the results. The detailed architecture of the proposed model is shown in Figure 3.

1) Input Embedding: Embedding is a commonly used technique in non-linear programming problems, which maps the sparse and high-dimensional word vectors into a low-dimensional space and vice versa. Initially, the input data, Euler angles $\theta_n = (\alpha_n, \beta_n, \gamma_n)$ and the actuator lengths $\xi_i = [l_1, l_2, l_3, l_4]$ are normalized and combined in Eq. (9) to form the input matrix $\mathbf{X} \in \mathbb{R}^{j\times d}$ as:

$$\mathbf{X} = \begin{bmatrix} \theta_{1,\alpha} & \theta_{1,\beta} & \theta_{1,\gamma} & \xi_{1,1} & \xi_{1,2} & \xi_{1,3} & \xi_{1,4} \\ \theta_{2,\alpha} & \theta_{2,\beta} & \theta_{2,\gamma} & \xi_{2,1} & \xi_{2,2} & \xi_{2,3} & \xi_{2,4} \\ \vdots & \vdots & \vdots & \vdots & \vdots & \vdots & \vdots \\ \theta_{n,\alpha} & \theta_{n,\beta} & \theta_{n,\gamma} & \xi_{n,1} & \xi_{n,2} & \xi_{n,3} & \xi_{n,4} \end{bmatrix} \tag{9}$$

here, $n = 4000$ is the number of data points and d is the dimension. In this work, the embedding mechanism is performed by the neural network's dense layers configured with 64 neurons and ReLU activation functions which map the input features into a 64-dimensional space to increase the representational capacity of the model.

2) Transformer Blocks: Following the embedding process, the features are passed into the series of Transformer blocks, composed of a multi-head self-attention mechanism and feed-forward network. The self-attention mechanism allows the model to weigh the importance of different parts (queries (Q), keys (K), and values (V)) of the input sequence (X) by computing the weighted sum of the values, where weights are determined by the attention scores generated by applying a softmax function to the compatibility scores of the queries and keys. These scores assess the importance of each value in

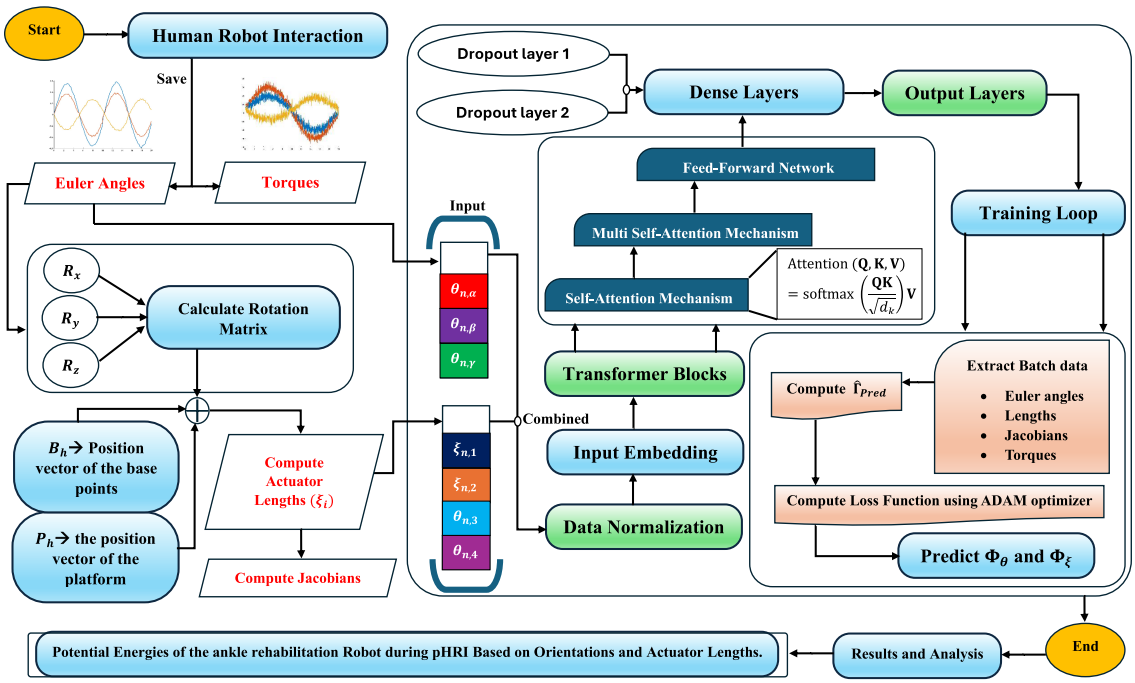

Fig. 3. The detailed summary of the input data and the proposed transformer model for the prediction of the potential energies of the parallel ankle rehabilitation robot during the human-robot interaction.

the final output, enabling the model to highlight relevant parts of the inputs. Furthermore, a linear transformation is applied to the concatenated outputs from all attention heads (each head learning different aspects of the input), forming the multi-head attention output and extending the model's ability to capture diverse patterns and dependencies.

After the last process, the output is passed through a feed-forward network (FFN) as outlined in Eq. (10), which consists of two linear transformations with ReLU activation function between them, which be given as

$$\mathrm{FFN}(X) = \max\left(0,\ X\ W_1 + b_1\right) W_2 + b_2, \tag{10}$$

Here, weights and biases are shown by W_1, W_2 and b_1, b_2 respectively. Following the self-attention and feed-forward steps, layer normalization is used to stabilize and accelerate the training process. Additionally, the dense layers configured with 128 neurons and dropout layers were incorporated to avoid overfitting by randomly assigning a portion of the input data to zero during the training process. The final transformation of the input data is expressed in Eq. (11) as:

$$\mathbf{X}_{\text{final}} = \text{Dropout}\left(\text{ReLU}\left(\mathbf{X}_{\text{transformed}}\,\mathbf{W}_{\text{dense}} + \mathbf{b}_{\text{dense}}\right)\right). \tag{11}$$

$\mathbf{X}_{\text{transformed}}$, $\mathbf{W}_{\text{dense}}$ and $\mathbf{b}_{\text{dense}}$ shows the output of the transformer block, weights and biases of the dense layers. Finally, the input data is processed into the output layer that consists of two separate fully connected layers for the unsupervised prediction of the potential energies by using the sigmoid activation function. The processed outputs in Eq. (12) are expressed as:

$$\begin{aligned}\Phi_\xi &= \sigma\left(\mathbf{X}_{\text{final}}\,\mathbf{W}_\xi + \mathbf{b}_\xi\right),\\ \Phi_\theta &= \sigma\left(\mathbf{X}_{\text{final}}\,\mathbf{W}_\theta + \mathbf{b}_\theta\right).\end{aligned} \tag{12}$$

where σ is the log-sigmoid activation function, $\mathbf{W}_\xi, \mathbf{W}_\theta$, $\mathbf{b}_\xi, \mathbf{b}_\theta$, are weights and biases of the output layer that needs to be determined using the training process.

3) Training Process: The training process of the above-mentioned transformer model involves feeding the input features into the model and optimizing the loss function, which is defined in terms of mean square error (MSE) between the predicted torque values $\hat{\Gamma}_{\text{pred}}$ derived using Eq. (7) and the actual torque values $\hat{\Gamma}_{\text{actual}}$ calculated during the experiment with stroke patients. The loss function Θ is given by Eq (13) as:

$$\Theta = \frac{1}{N}\sum_{i=1}^{N}\left(\hat{\Gamma}_{\text{actual},i} - \hat{\Gamma}_{\text{pred},i}\right)^2. \tag{13}$$

$N = 12000$ is the number of samples. To understand the effect of changes to the input parameters on the predicted outputs, the gradients of the loss with respect to the input features are calculated. Backpropagation is then employed to update the model's parameters using these gradients. The commonly used Adam optimizer is utilized to adaptively modify the learning rates for every parameter, improving the overall training procedure. The essential settings of the parameters involved in the designed model for the prediction of potential energies are dictated in Table II.

III. Results and Discussion

A. Transformer Model Evaluation

In this section, we present and analyze the results obtained by applying the proposed transformer model on the experimental data of the stroke patients to predict the potential energies Φ_θ and Φ_ξ of the ankle rehabilitation robot during the physical human-robot interaction. Initially, we performed

TABLE II
SETTING OF THE IMPORTANT PARAMETERS INVOLVED IN THE DESIGNED TRANSFORMER MODEL

Parameter	Setting	Parameter	Setting
Embedding Dimension	64	Transformer Blocks	4
Number of Heads	4	Dropout Rate	0.2
Feed-Forward Dimension	128	Optimizer	Adam
Learning Rate	0.001	Loss Function	MSE
Batch Size	32	Number of Epochs	1000

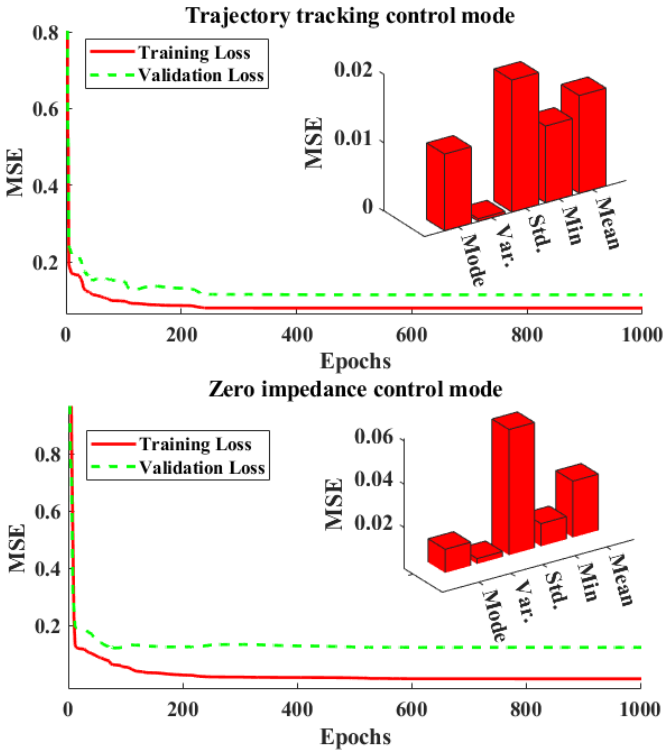

Fig. 4. The training loss and validation loss of the proposed model and the statistics of training loss (MSE) calculated during 1000 epochs for the prediction of Φ_θ and Φ_ξ for the data averaged over five stroke patients.

a series of experiments to determine the optimal parameter settings for the designed model by varying the hyperparameters like batch size $(16, 32, 64, 128)$, learning rate $(1 \times 10^{-5}$ to $1 \times 10^{-2})$, number of epochs $(200, 500, 1000, 1500)$, neurons $(32, 64, 128, 256)$, and number of transformer blocks $(1, 2, 4, 6)$. Through the detailed sensitivity analysis, the model with a batch size of 32, a learning rate of 0.001, and 1000 epochs with 4 transformer blocks provides the most suitable balance between the convergence rate and stability of the model. The performance of the model was assessed by plotting the loss values (training loss and validation loss) against each epoch in Figure 4 during the learning process in both the trajectory tracking control mode and the zero impedance control mode. The error starts high at around 1.1 and rapidly decreases within the first 200 epochs, which indicates fast learning and effective error minimization by the model. Additionally, the bar graph inside the performance plot shows the statistics of the indices used to measure the performance of the training loss, including the minimum, mean, standard deviation, variance, and mode of the results. The values of these indices in the training loss for potential energies with trajectory tracking control mode are less than the training loss for the zero impedance control mode. It is worth noticing that the values of the statistical measures are close to zero, reflecting the perfect modeling of the predicted results.

B. Transactive Energy

It is important to understand the role of transactive energy in the rehabilitation process of stroke patients. It refers to the process by which stored potential energy is transformed into kinetic energy and drives movement of the patient's ankle joint. The potential energy is stored in the actuators through configurations involving elastic deformation. When the robot initiates movement, it transforms the stored potential energy into kinetic energy, enabling the robot to exert the necessary forces and torques on the patient's ankle which assists patients in moving their ankle joints through various ranges of motion along IN/EV, DO/PL, and AD/AB.

Stroke patients struggle with significant neuromuscular deficits, including weakened muscle control, spasticity, and coordination issues. These problems make it difficult and hinder their ability to generate and sustain the potential energy necessary for effective movement, increasing their reliance on robotic assistance. Determining the potential energies in such a complex human-robot interaction is difficult. Therefore, to address these issues, it is essential to understand and manage the potential energies involved in the rehabilitation process. There are primarily two types of potential energy from the robot's perspective: the potential energy due to the robot's orientation (Φ_θ), which depends on its stiffness and alignment, and the potential energy arising from joint stiffness and the joint's position (Φ_ξ) of the robot. To accurately determine these potential energies with precision is complex because of their high dimensionality and the continuous changes in the state and action space of both the robot and the patient.

In this work, we have utilized the transformer model to capture the high-dimensional characteristics for the energy estimation during the interaction of five stroke patients with the ankle rehabilitation robot by using the predefined trajectories, configurations of the elastic deformation of the actuators, and the applied torques. Figure 5(a) and (b) shows the potential energy due to the robot's orientation (Φ_θ), and the potential energy due to joints position (Φ_ξ) of the ankle rehabilitation robot with impedance controller operated in two modes, trajectory tracking control mode, and zero impedance control mode respectively. The results illustrate the comparison between the designed transformer model (solid black line) and those made by Long Short-Term Memory (LSTM) type of recurrent neural networks (dashed red line) and convolutional neural networks (dotted blue line). All models were trained using the parameters settings given in Table II and III. To ensure a fair comparison, the parameters such as learning rate, number of epochs, dense layer units, dropout layer and optimizer were kept consistent across all models. The transformer model due to its unique architecture, which excels in handling temporal dependencies and modeling long-range interactions within the data provides more accurate predictions of the energy

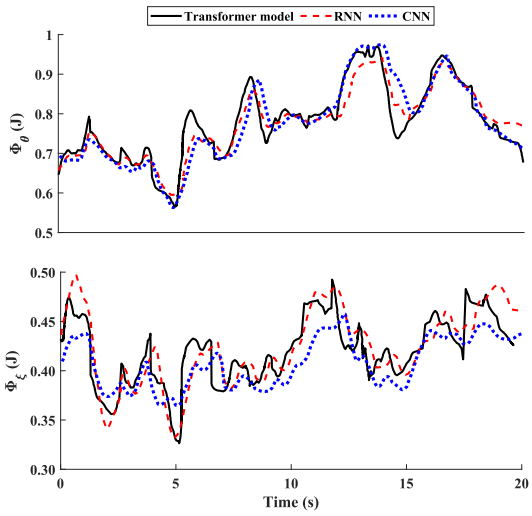

(a)

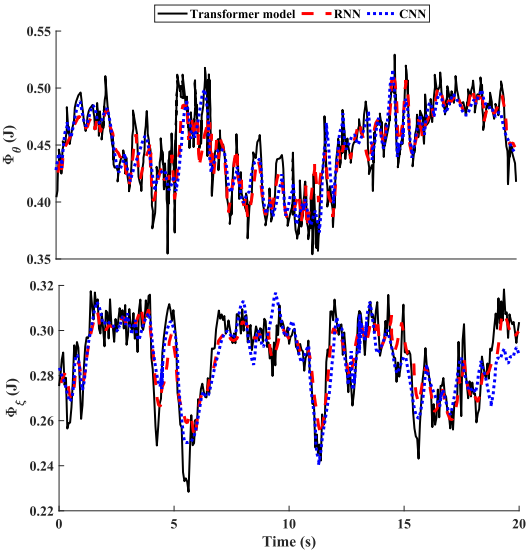

(b)

Fig. 5. The behavior of the potential energies in Cartesian space and joint space during the energy transfer between stroke patients (averaged over five patients) and the ankle rehabilitation robot with the impedance controller operated in (a) trajectory tracking control mode and (b) zero impedance control mode. The results also show the comparison of the predicted energies by the designed Transformer model with the other models like RNN and CNN.

dynamics as it closely tracks the actual energy values (as is evident from the small fluctuations and finer variations of the energy levels) over time. The RNN and CNN models follow a similar general trend as the transformer model, but they exhibit limitations in capturing the detailed variations. These models either oversmooth or fail to accurately represent the energy changes, especially in regions where sharp fluctuations occur. It is concluded that the transformer model is a more reliable tool for predicting energy dynamics in both active and passive modes, ensuring better-informed decisions for the rehabilitation process and optimizing patient outcomes. The comparative analysis of the performance values, and computational complexity of the techniques are shown in Table IV.

TABLE III
HYPER-PARAMETERS SETTING FOR THE EXECUTION OF CNN AND RNN (LSTM) MODELS

Parameter	CNN Model	RNN (LSTM) Model
Layer 1 Type	Conv1D (64 filters, kernel size = 3)	LSTM (64 units)
Layer 2 Type	Conv1D (128 filters, kernel size = 2)	LSTM (128 units)
Dense Layer Units	128	128
Dropout Rate	0.2	0.2
Optimizer	Adam	Adam
Learning Rate	0.001	0.001
Epochs	1000	1000

TABLE IV
COMPARISON OF TRANSFORMER, RNN, AND CNN MODELS FOR ENERGY PREDICTION

Metric	Transformer Model	RNN	CNN
Training Loss (MSE) (Active Mode)	0.0013	0.0986	0.0956
Training Loss (MSE) (Passive Mode)	0.0021	0.0529	0.0913
Accuracy in Capturing Small Variations	High	Medium	Low
Computation Time (s)	1980 (s)	1261 (s)	1083 (s)

Furthermore, in the trajectory tracking control mode, the robot's actuators perform most of the work and fully control the movement of the patient's ankle joint, guiding it along predefined paths. In this case, values of the predicted potential energies (Φ_ξ) and (Φ_θ) ranges from 0.3 to 0.5 Joules and 0.55 to 1 Joule. The same trends and ranges of the energy values were observed by Lachner et al. [32] for the safe robot behavior during the physical human-robotic interaction. The higher and more stable level of the values of potential energies ensures that the robot is consistently applying the necessary forces to move the joint through the desired trajectories. In zero impedance control mode, the potential energy is attributed to the combined efforts of the muscles of patients and the robot's actuators. The kinetic energy produced by the muscles is partly transformed into potential energy that is stored in the actuators of the robot which is used to help the patient in completing the movements and offers a responsive and adaptable therapy. It is observed that the energies (Φ_ξ) and (Φ_θ) in trajectory tracking control mode are higher than the zero impedance control mode, as it exerts additional force to assist and navigate the stroke patient along the particular predefined trajectories and overcome both the mechanical resistance of the robot and the inertia of the patient's limb. In addition, Figure 6 presents the results as an average over multiple trials of experiments for the stroke patients, depicted with a mean line and an accompanying $\pm$ standard deviation shaded area. This visualization provides a representation of the central tendency of the potential energies while capturing the variability across trials. The mean standard deviation lies around 0.0143 (J), 0.0174 (J) and 0.0253 (J), 0.0462 (J), for the potential energies in Cartesian space and joint space during the trajectory tracking control mode and zero impedance control mode.

Moreover, the energy behavior (Φ_θ) for both the passive and active modes across different ranges of motion are shown in Figure 7. In trajectory tracking control mode, the values of energy peak are observed around the extreme values because of the displacement from the neutral positions showing the significant elastic and gravitational energy storage resulting in higher and more variable energy due to the robot's control

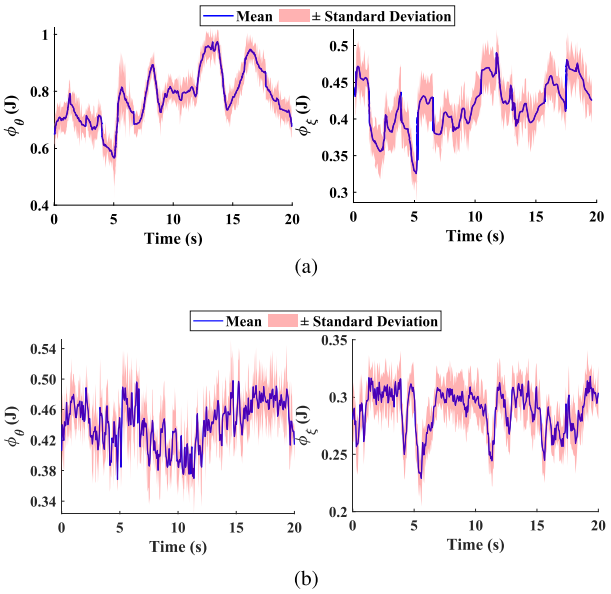

Fig. 6. Mean ± standard deviation of multiple trial results for the potential energies in Cartesian space and joint space during the energy transfer between stroke patients (averaged over five patients) and the ankle rehabilitation robot with the impedance controller operated in (a) trajectory tracking control mode and (b) zero impedance control mode.

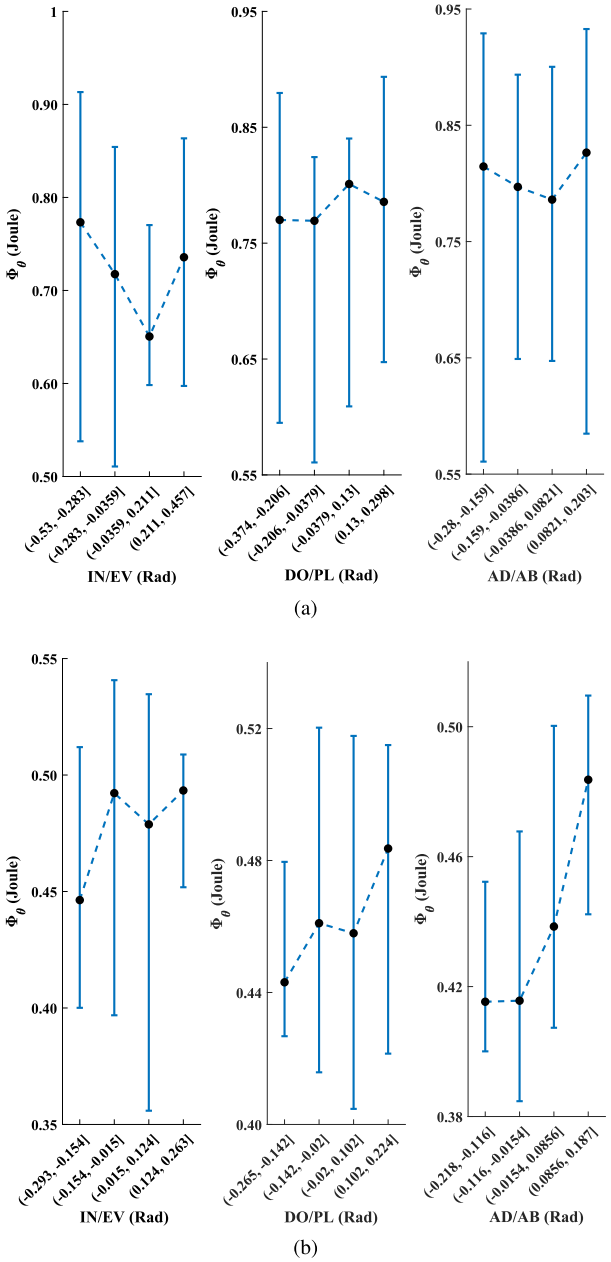

Fig. 7. Mean values with the bars showing maximum and minimum values of potential energies due to the orientation based on the (a) trajectory tracking control mode and (a) zero impedance control mode of the controller during the pHRI averaged over five stoke patients.

over movement. In zero impedance control mode, the values of (Φ_θ) are slightly lower than in the trajectory tracking control mode, due to the active participation of the patient and the supportive role of the ankle rehabilitation robot. It is observed that the (Φ_θ) remains consistent showing the smoother transitions of movement and effectiveness of the rehabilitation robot in patient recovery. Finally, we have studied the influence of variations in the lengths of the individual actuator on the potential energy due to joint positions (Φ_ξ) of the ankle rehabilitation robot during the active and passive modes. Figure 8 (a) shows that the highest value for (Φ_ξ) was observed in the middle to higher length ranges indicating greater displacement and energy storage due to the robot's control over movement. In the case of active mode Figure 8 (b), the values of (Φ_ξ) are lower across all the actuators, reflecting the active engagement of the patient and reduced resistance from the robot.

In addition to the energy transfer dynamics from the robot to the human, we have computed the energy exerted by the human on the robot in the form of work done as shown in Figure 9. In the trajectory tracking control mode, the robot is responsible for moving the human ankle along a predefined trajectory so essentially the work done by the human on the robot should be zero. However, we expect substantial nonpassive behavior from persons with neurological impairment, since the damage to the neural pathways may significantly affect their central as well as peripheral neural networks to cause nonpassive behavior due to altered feedback [49]. In the zero impedance control mode, the robot minimizes its resistance to the human's movements, allowing the human to control and initiate the movements actively. The results of this mode illustrate a more dynamic interaction, with the work done by the human on the robot displaying greater variability and higher magnitudes compared to the trajectory tracking control mode as shown in Table V. The values of the work done by stroke patients range between −0.5 and 1 Joules with a standard deviation of 0.3861 Joule, highlighting the active engagement of the human muscles to apply sufficient forces to guide the ankle rehabilitation robot. Moreover, the work done by the patients during the rehabilitation exercise is directly correlated with the potential energies in the Cartesian and joint space of the ankle rehabilitation robot. The lower values of the work done in the passive mode correlate with the higher potential energy stored in the robot. In contrast, the potential energies are lower when the patient actively contributes to the movement and the work done by the patient increases,

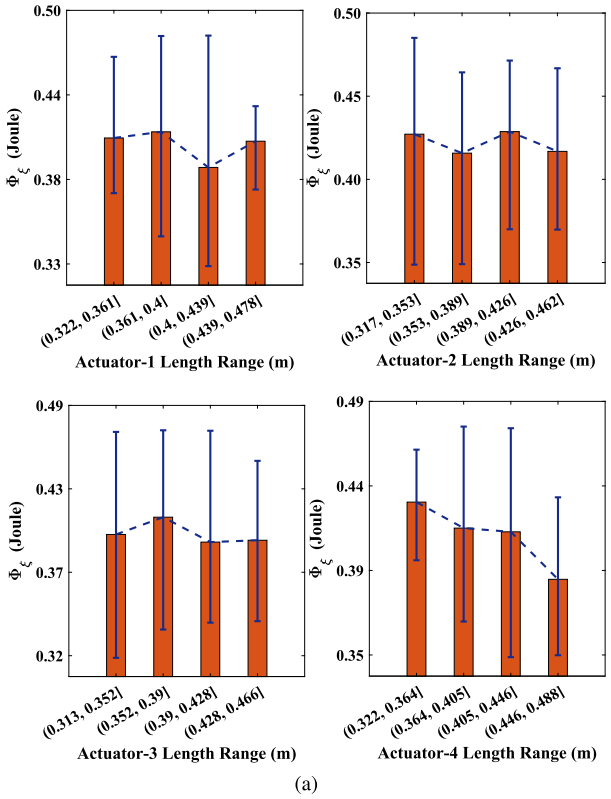

Fig. 8. Impact of the actuator lengths on Φ_ξ during the pHRI averaged over five stroke patients for (a) trajectory tracking control mode and (b) zero impedance control mode of the impedance controller. The bar graph shows the mean values while the bars at the extreme highlight the maximum and minimum values of Φ_ξ.

reflecting the patient's effort to generate movement, which is important for strengthening muscles and recovery.

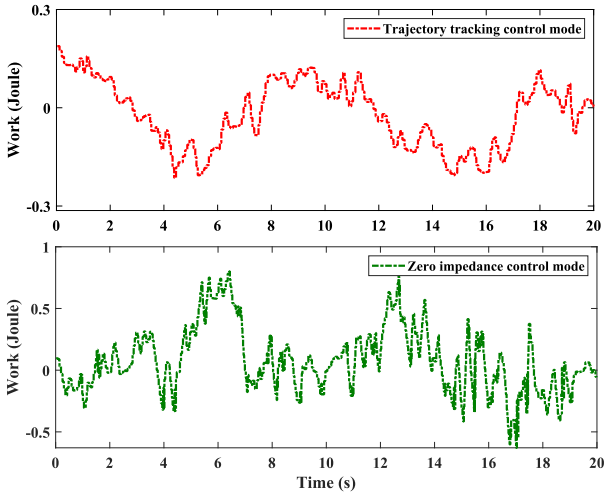

Fig. 9. Work done by the stroke patients (averaged over five subjects) on the ankle rehabilitation robot during physical human-robot interaction in different control modes.

TABLE V
STATISTICS OF THE WORK DONE (JOULE) BY THE STROKE PATIENTS (AVERAGE OF FIVE PATIENTS) ON A ROBOT DURING THE INTERACTION IN DIFFERENT CONTROL MODES

Work done (Joule)					
Trajectory tracking control mode			Zero impedance control mode		
Mean	Std	Total Work done	Mean	Std	Total Work done
0.1031	0.0962	3.9767	0.5024	0.3861	9.9249

The results demonstrate that transactive energy regulation between the human and the exoskeleton holds significant potential for improving stroke ankle rehabilitation. This regulation ensures that the robotic system provides appropriate assistance while encouraging patient effort. In stroke rehabilitation, optimizing the balance between patient effort and robotic support is important. When the patient actively participates in movement, reducing the exoskeleton's energy which encourages muscle activation and neuromuscular recovery, fostering greater independence over time. Conversely, in cases where the patient has limited motor control, the exoskeleton can provide more energy to assist in movement without overwhelming the patient, thus preventing fatigue and disengagement. By understanding the transactive energy flow, therapists and clinicians can better tune the robot's control algorithms to the individual specific needs encouraging the patient to progressively take on more responsibility for movement, which strengthens muscles and accelerates recovery while reducing dependence on robotic support.

IV. CONCLUSION

This paper introduces the concept of transactive energy to establish a robust framework for capturing the energy interactions between stroke patients and the ankle rehabilitation robot. The transformer-based model is implemented to accurately predict potential energies dissipated from the robot in both trajectory tracking control mode and zero impedance control mode, offering a robust, coordinate-invariant framework for managing energy transfer. In the trajectory tracking control mode, the robot exerts significant control over the movement,

resulting in higher potential energy dissipation and leading to minimal work done by the human on the robot. Conversely, in the zero impedance control mode, the robot minimizes its resistance to allow the human to take the lead in initiating and controlling movements. This results in lower potential energy dissipation within the robot, as its actuators are less engaged. Furthermore, across multiple trials with stroke patients, the potential energy levels predicted by the designed transformer model in both Cartesian and joint spaces during both control modes demonstrate consistency, with mean standard deviations of approximately 0.0143 (J), 0.0174 (J), 0.0253 (J), and 0.0462 (J). Simultaneously, the work done by the human is significantly higher and more variable, reflecting the active effort of the patient's ankle to drive the movements. By minimizing the impedance of the robot and encouraging the patient's active engagement, the rehabilitation process reflects enhanced muscle strength towards overall recovery which aligns with the goal of rehabilitation, where the human subject's energy dissipation should increase over time for independence and reduced reliance on robotic assistance. These results highlight the potential of transactive energy concepts to design more effective and patient-centered rehabilitation protocols, ultimately improving therapeutic outcomes.

In the future, we aim to extend the present work by considering the artificial potential energy of the environment and gravitational potential energy during the physical human-robotic interaction. Also, we will develop an energy-based controller to optimize and control HRI by modulating transactive energy in order to enhance efficiency and effectiveness of the rehabilitation process.

REFERENCES

[1] W. Ling, "Energy optimization of a wearable lower limb rehabilitation robot based on deep learning," *Sustain. Energy Technol. Assessments*, vol. 56, Mar. 2023, Art. no. 103123.

[2] T. Zhou, C. Xiong, J. Zhang, W. Chen, and X. Huang, "Regulating metabolic energy among joints during human walking using a multiarticular unpowered exoskeleton," *IEEE Trans. Neural Syst. Rehabil. Eng.*, vol. 29, pp. 662–672, 2021.

[3] D. Zeng, Y. Liu, C. Qu, J. Cong, Y. Hou, and W. Lu, "Design and human–robot coupling performance analysis of flexible ankle rehabilitation robot," *IEEE Robot. Autom. Lett.*, vol. 9, no. 1, pp. 579–586, Jan. 2024.

[4] S. M. Cobian-Aquino et al., "Adaptive state restricted barrier Lyapunov-based control of a stewart platform used as ankle-controlled mobilizer," *ISA Trans.*, vol. 148, pp. 435–448, May 2024.

[5] R. Karakis, K. Gurkahraman, G. D. Mitsis, and M.-H. Boudrias, "Deep learning prediction of motor performance in stroke individuals using neuroimaging data," *J. Biomed. Inf.*, vol. 141, May 2023, Art. no. 104357.

[6] M. J. Girone, G. C. Burdea, and M. Bouzit, "The 'rutgers ankle' orthopedic rehabilitation interface," in *Proc. ASME Int. Mech. Eng. Congr. Expo.*, vol. 16349, 1999, pp. 305–312.

[7] P. S. Lum, C. G. Burgar, M. V. D. Loos, P. C. Shor, M. Majmundar, and R. Yap, "MIME robotic device for upper-limb neurorehabilitation in subacute stroke subjects: A follow-up study," *J. Rehabil. Res. Develop.*, vol. 43, no. 5, p. 631, 2006.

[8] N. A. Khan, S. Hussain, W. Spratford, R. Goecke, K. Kotecha, and P. K. Jamwal, "Deep learning-driven analysis of a six-bar mechanism for personalized gait rehabilitation," *J. Comput. Inf. Sci. Eng.*, vol. 25, no. 1, pp. 1–23, Jan. 2025.

[9] N. F. J. Waterval et al., "Stiffness-optimized ankle-foot orthoses improve walking energy cost compared to conventional orthoses in neuromuscular disorders: A prospective uncontrolled intervention study," *IEEE Trans. Neural Syst. Rehabil. Eng.*, vol. 28, no. 10, pp. 2296–2304, Oct. 2020.

[10] D. M. Yadav, "Application of technologies robotic rehabilitation in children with upper limb injury," *Int. J. Preventive Med. Health*, vol. 1, no. 4, pp. 1–5, Sep. 2021.

[11] A. Roy et al., "Measurement of human ankle stiffness using the anklebot," in *Proc. IEEE 10th Int. Conf. Rehabil. Robot.*, Jun. 2007, pp. 356–363.

[12] J. Bae et al., "A lightweight and efficient portable soft exosuit for paretic ankle assistance in walking after stroke," in *Proc. IEEE Int. Conf. Robot. Autom. (ICRA)*, May 2018, pp. 2820–2827.

[13] Y. Huo, M. N. Khan, Z. F. Shao, and Y. Pan, "Development of a novel cable-driven parallel robot for full-cycle ankle rehabilitation," *Mechatronics*, vol. 101, Aug. 2024, Art. no. 103210.

[14] T.-C. Chang and X.-D. Zhang, "Kinematics and reliable analysis of decoupled parallel mechanism for ankle rehabilitation," *Microelectron. Rel.*, vol. 99, pp. 203–212, Aug. 2019.

[15] J. Zhao, T. Yang, X. Sun, J. Dong, Z. Wang, and C. Yang, "Sliding mode control combined with extended state observer for an ankle exoskeleton driven by electrical motor," *Mechatronics*, vol. 76, Jun. 2021, Art. no. 102554.

[16] D. R. Lee, Y. K. Shin, J.-H. Park, and J. H. You, "Concurrent validity and test-retest reliability of the walkbot-k system for robotic gait training," *J. Mech. Med. Biol.*, vol. 16, no. 8, Dec. 2016, Art. no. 1640029.

[17] J. Arnold and H. Lee, "Variable impedance control for pHRI: Impact on stability, agility, and human effort in controlling a wearable ankle robot," *IEEE Robot. Autom. Lett.*, vol. 6, no. 2, pp. 2429–2436, Apr. 2021.

[18] J. C. Pérez-Ibarra, A. A. G. Siqueira, M. A. Silva-Couto, T. L. de Russo, and H. I. Krebs, "Adaptive impedance control applied to robot-aided neuro-rehabilitation of the ankle," *IEEE Robot. Autom. Lett.*, vol. 4, no. 2, pp. 185–192, Apr. 2019.

[19] J. Zhang, J. Lin, V. Peddinti, and R. D. Gregg, "Optimal energy shaping control for a backdrivable hip exoskeleton," in *Proc. Amer. Control Conf. (ACC)*, May 2023, pp. 2065–2070.

[20] K. Qian, Z. Zhang, S. Chakrabarty, and S. Xie, "Iterative impedance learning control for ankle rehabilitation," in *Proc. 27th Int. Conf. Mechatronics Mach. Vis. Pract. (M2VIP)*, Nov. 2021, pp. 492–497.

[21] J. I. Han, J.-H. Lee, H. S. Choi, J.-H. Kim, and J. Choi, "Policy design for an ankle-foot orthosis using simulated physical human–robot interaction via deep reinforcement learning," *IEEE Trans. Neural Syst. Rehabil. Eng.*, vol. 30, pp. 2186–2197, 2022.

[22] Z. Li, W. Shang, and B. Zhang, "Hybrid impedance control of cable-driven parallel robots using adaptive friction compensation," *IEEE Trans. Ind. Electron.*, vol. 72, no. 1, pp. 703–713, Jan. 2025.

[23] C. Wang et al., "Research on an ankle joint auxiliary rehabilitation robot with a rigid-flexible hybrid drive based on a 2-s' ps' mechanism," *Appl. Bionics Biomech.*, vol. 2019, no. 1, 2019, Art. no. 7071064.

[24] B. Abayneh, "Design and simulation of fuzzy-based nonlinear-PID and sliding mode controllers for ankle rehabilitation soft wearable robot," *Int. J. Biomechtron. Biomed. Robot.*, vol. 4, no. 1, pp. 1–12, 2022.

[25] J. Lee, M. Kim, and K. Kim, "A control scheme to minimize muscle energy for power assistant robotic systems under unknown external perturbation," *IEEE Trans. Neural Syst. Rehabil. Eng.*, vol. 25, no. 12, pp. 2313–2327, Dec. 2017.

[26] J. E. Colgate and N. Hogan, "Robust control of dynamically interacting systems," *Int. J. Control*, vol. 48, no. 1, pp. 65–88, 1988.

[27] B. Li, X. Li, H. Gao, and F.-Y. Wang, "Advances in flexible robotic manipulator systems—Part I: Overview and dynamics modeling methods," *IEEE/ASME Trans. Mechatronics*, vol. 29, no. 2, pp. 1100–1110, Apr. 2024.

[28] H. Lee and N. Hogan, "Energetic passivity of the human ankle joint," *IEEE Trans. Neural Syst. Rehabil. Eng.*, vol. 24, no. 12, pp. 1416–1425, Dec. 2016.

[29] M. Yeatman and R. D. Gregg, "Using energy shaping and regulation for limit cycle stabilization, generation, and transition in simple locomotive systems," *J. Comput. Nonlinear Dyn.*, vol. 16, no. 9, Sep. 2021, Art. no. 091005.

[30] J. Lin, G. C. Thomas, N. V. Divekar, V. Peddinti, and R. D. Gregg, "A modular framework for task-agnostic, energy shaping control of lower limb exoskeletons," *IEEE Trans. Control Syst. Technol.*, vol. 32, no. 6, pp. 2359–2375, Nov. 2024.

[31] J. Lin, R. D. Gregg, and P. B. Shull, "Improving task-agnostic energy shaping control of powered exoskeletons with task/gait classification," *IEEE Robot. Autom. Lett.*, vol. 9, no. 8, pp. 6848–6855, Aug. 2024.

[32] J. Lachner, F. Allmendinger, E. Hobert, N. Hogan, and S. Stramigioli, "Energy budgets for coordinate invariant robot control in physical human–robot interaction," *Int. J. Robot. Res.*, vol. 40, nos. 8–9, pp. 968–985, Aug. 2021.

[33] A. Dietrich, C. Ott, and S. Stramigioli, "Passivation of projection-based null space compliance control via energy tanks," *IEEE Robot. Autom. Lett.*, vol. 1, no. 1, pp. 184–191, Jan. 2016.

[34] V. L. Asv, S. K. Mangipudi, and R. R. Manyala, "Control constraint-based optimal pid-pss design for a widespread operating power system using SAR algorithm," *Int. Trans. Electr. Energy Syst.*, vol. 31, no. 12, 2021, Art. no. e13146.

[35] M. F. Shah, S. Hussain, R. Goecke, and P. K. Jamwal, "Mechanism design and control of shoulder rehabilitation robots: A review," *IEEE Trans. Med. Robot. Bionics*, vol. 5, no. 4, pp. 780–792, Nov. 2023.

[36] M. E. Basiri, S. Nemati, M. Abdar, E. Cambria, and U. R. Acharya, "ABCDM: An attention-based bidirectional CNN-RNN deep model for sentiment analysis," *Future Gener. Comput. Syst.*, vol. 115, pp. 279–294, Feb. 2021.

[37] J. Su, M. Ahmed, Y. Lu, S. Pan, W. Bo, and Y. Liu, "RoFormer: Enhanced transformer with rotary position embedding," *Neurocomputing*, vol. 568, Feb. 2024, Art. no. 127063.

[38] P. K. Jamwal, S. Q. Xie, S. Hussain, and J. G. Parsons, "An adaptive wearable parallel robot for the treatment of ankle injuries," *IEEE/ASME Trans. Mechatronics*, vol. 19, no. 1, pp. 64–75, Feb. 2014.

[39] P. K. Jamwal, S. Hussain, M. H. Ghayesh, and S. V. Rogozina, "Impedance control of an intrinsically compliant parallel ankle rehabilitation robot," *IEEE Trans. Ind. Electron.*, vol. 63, no. 6, pp. 3638–3647, Jun. 2016.

[40] P. K. Jamwal, S. Hussain, and S. Q. Xie, "Three-stage design analysis and multicriteria optimization of a parallel ankle rehabilitation robot using genetic algorithm," *IEEE Trans. Autom. Sci. Eng.*, vol. 12, no. 4, pp. 1433–1446, Oct. 2015.

[41] P. K. Jamwal and S. Hussain, "Multicriteria design optimization of a parallel ankle rehabilitation robot: Fuzzy dominated sorting evolutionary algorithm approach," *IEEE Trans. Syst., Man, Cybern. Syst.*, vol. 46, no. 5, pp. 589–597, May 2016.

[42] P. K. Jamwal, S. Hussain, Y. H. Tsoi, M. H. Ghayesh, and S. Q. Xie, "Musculoskeletal modelling of human ankle complex: Estimation of ankle joint moments," *Clin. Biomech.*, vol. 44, pp. 75–82, May 2017.

[43] B. Siciliano, L. Sciavicco, L. Villani, and G. Oriolo, *Force Control*. Cham, Switzerland: Springer, 2009.

[44] S. Stramigioli, *Modeling and IPC Control of Interactive Mechanical Systems-A Coordinate-free Approach*. Cham, Switzerland: Springer, 2001.

[45] F. Caccavale, C. Natale, B. Siciliano, and L. Villani, "Six-DOF impedance control based on angle/axis representations," *IEEE Trans. Robot. Autom.*, vol. 15, no. 2, pp. 289–300, Apr. 1999.

[46] C. Ott, *Cartesian Impedance Control of Redundant and Flexible-joint Robots*. Cham, Switzerland: Springer, 2008.

[47] P. K. Jamwal, S. Hussain, M. H. Ghayesh, and S. V. Rogozina, "Adaptive impedance control of parallel ankle rehabilitation robot," *J. Dyn. Syst., Meas., Control*, vol. 139, no. 11, Nov. 2017, Art. no. 111006.

[48] A. Vaswani et al., "Attention is all you need," in *Proc. Adv. Neural Inf. Process. Syst.*, vol. 30, Jun. 2017, pp. 5998–6008.

[49] V. Dietz and T. Sinkjaer, "Spastic movement disorder: Impaired reflex function and altered muscle mechanics," *Lancet Neurol.*, vol. 6, no. 8, pp. 725–733, Aug. 2007.